
Title: Fabrication of small aspheric moulds using single point inclined axis grinding

Author: Fengjun Chen Shaohui Yin Han Huang Hitoshi Ohmori

PII: S0141-6359(14)00136-6
DOI: http://dx.doi.org/doi:10.1016/j.precisioneng.2014.06.009
Reference: PRE 6142

To appear in: *Precision Engineering*

Received date: 22-7-2013
Revised date: 19-5-2014
Accepted date: 21-6-2014

Please cite this article as: Chen F, Yin S, Huang H, Ohmori H, Fabrication of small aspheric moulds using single point inclined axis grinding, *Precision Engineering* (2014), http://dx.doi.org/10.1016/j.precisioneng.2014.06.009

# Fabrication of small aspheric moulds using single point inclined axis grinding

Fengjun Chen[a,*], Shaohui Yin[a], Han Huang[b], Hitoshi Ohmori[c]

[a]National Engineering Research Centre for High Efficiency Grinding, Hunan University, Changsha, 410082, PR China

[b]School of Mechanical and Mining Engineering, The University of Queensland, QLD4072, Australia

[c] The Institute of Physical and Chemical Research (RIKEN), Saitama, 351-0198, Japan

*Corresponding authors
Email addresses: *abccfj@126.com* (Fengjun Chen). Tel.: +86 731 88829817; fax: +86 731 88823912

# Fabrication of small aspheric moulds using single point inclined axis grinding

**Abstract**

Single point inclined axis grinding techniques, including the wheel setting, wheel-workpiece interference, error source determination and compensation approaches, were studied to fabricate small aspheric moulds of high profile accuracy. The interference of a cylindrical grinding wheel with the workpiece was analysed and the criteria for selection of wheel geometry for avoiding the interference was proposed. The grinding process was performed with compensation focused on two major error sources, wheel setting error and wheel wear. The grinding results showed that the compensation approach was efficient and the developed grinding process was capable to generate small aspheric concave surfaces on tungsten carbide material with a profile error of smaller than 200 nm in PV value after two to three compensation cycles.

***Keywords:*** single point grinding, inclined axis, compensation, profile error, aspheric mould

## 1. Introduction

Meso and micro optical components have been extensively used in a wide range of industrial applications, such as aerospace, optics, photonics and telecommunications, in the past decade [1,2]. With the further progress in modern industries, the requirement for high precision and the demand for mass production of those components are considerably increased [3,4]. As a result, a great research effort has been directed toward the development of high precision grinding processes for optical products, especially in aspheric form, in recent years [5,6]. For example, Chen et al. developed a parallel grinding protocol to generate micro aspheric mould inserts [7]. Cha et al. carried out a study of the optimization of grinding conditions to improve surface roughness and profile accuracy of aspheric glass lenses for phone camera [8]. Han et al. specially designed an evolutionary grinding process for the fabrication of aspheric surfaces of a glass ceramic substrate [9]. Kim et al. developed a new sub-micron control algorithm in order to interpolate tool path in grinding and polishing aspheric surfaces [10]. To improve the profile accuracy through reducing the effects of tool fabrication and positioning errors and tool wear, several techniques for precise truing and dressing grinding wheels were developed [11-14], in-process measuring methods for form errors was employed [5,15] and a number of compensation approaches for tooling errors [16-18], tool wear [19-21], machine tool geometric error [22,23] and thermal effect [24,25] were proposed.

Nevertheless, there are still several key problems that need to be further addressed. For instance, the quality of truing and dressing of grinding wheels and tool wear had such significant effect on the profile accuracy of the ground surface [16-19], so that the compensation algorithm for such errors must be more efficient and rigorous. It was

difficult to determine precisely the contact point of the arc grinding wheel during grinding [16], therefore, the accuracy of the compensated tool path was affected and the compensation efficiency in the next grinding cycle was compromised. Also, the error sources usually have interacted impact on the machined profile accuracy, the error should be compensated based on the existing machine [23] and on-machine measurement [15] should be encouraged in order to improve the compensation efficiency.

In this paper, we report a single point inclined axis nanogrinding protocol and its on-machine error compensation method. In this grinding protocol, a cylindrical superfine grinding wheel was selected and the grinding was carried out by integrating a rotary movement around *B*-axis into the conventionally used *X* and *Z* linear movements of a wheel. This enabled the single point contact during the entire grinding process. Error compensation approach was also developed, with the focus on centring error and tool wear error.

## 2. Set-up and characteristics of single point inclined axis grinding mode

As shown in Fig. 1(a), in conventional perpendicular arc envelope grinding, the wheel spindle is parallel to *Y*-axis, while the workpiece spindle is parallel to *Z*-axis. Because the rotational axis of the grinding wheel is perpendicular to that of the work-piece, the wheel will interfere with the workpiece if the sag of the concave surface.

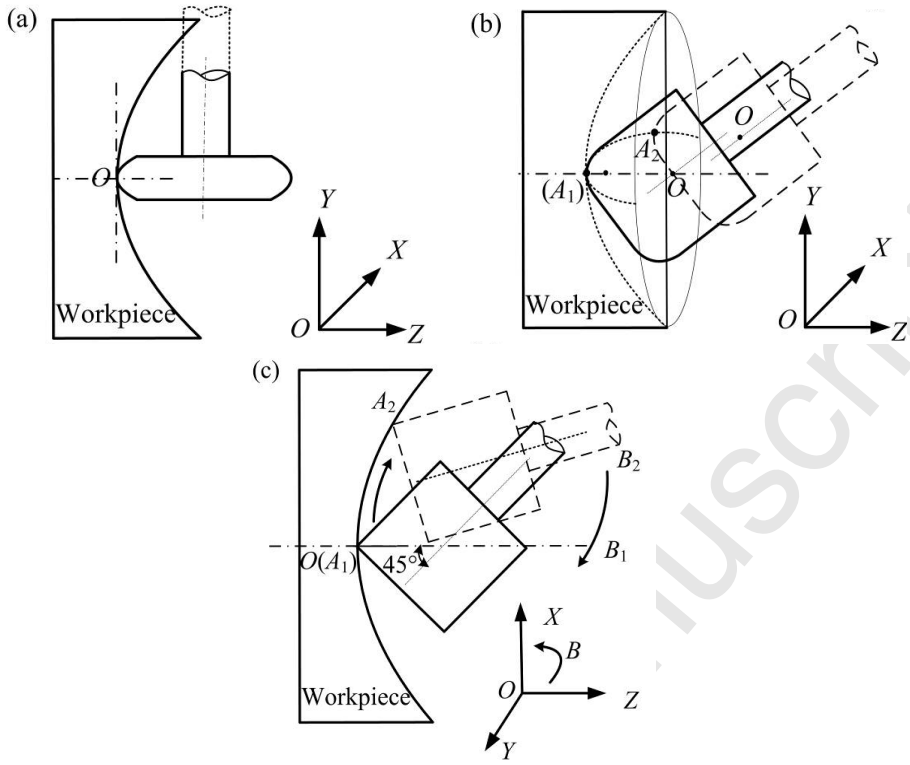


Fig. 1: Schematic illustration of three different grinding modes: (a) perpendicular mode, (b) inclined axis mode using an arc wheel and (c) single point inclined axis mode.

being ground is too great. Therefore, this method is mainly used in machining aspheric surface of relatively large apertures. To avoid the interference, the wheel axis can be inclined, as shown in Fig. 1(b), where the wheel and work spindles intersect at a certain angle of normally 45°. In arc grinding shown in Figs. 1(a) and 1(b) the wheel arc is in contact with the workpiece, so the profile accuracy of the arc grinding wheel has significant effect on the profile accuracy of the ground surface. Also, the contact point is varied (moving along the arc) during arc grinding, so it is difficult to accurately estimate the wheel wear and hence lead to the inaccuracy in determine the tool path for next grinding cycle.

To solve the abovementioned problems, in this work we proposed: (1) to adopt the inclined wheel spindle mode to effectively avoid interference between the wheel and the workpiece for grinding micro/meso optical surfaces, and (2) to use a cube corner wheel,

instead of a arc corner wheel, in order to maintain a single contact point during grinding. Fig. 1(c) shows the set-up of the grinding wheel and workpiece. It should be noted that although it is still inclined axis grinding, the inclined angle of the grinding spindle varies with the location of the contact point, i.e. a rotary movement around *B*-axis is added into the movements of the wheel along *X* and *Z* axes that occurs in the conventional arc grinding. The advantages for using this set-up are summarised as follows.

- Through controlling the movements along *X*-*Z*-*B* axes, the grinding points can be kept at the rotational centre of *B*-axis, so the chance for the wheel-workpiece interference is minimised. In other words, relatively large wheels can be selected.
- As the contact between the wheel and the workpiece is a point, so the accuracy for determining the grinding path is increased. This makes the subsequent compensation relatively easy.
- It is much easier to obtain the sharp corner through truing the end and cylindrical surfaces of a grinding wheel (in linear movement along one axis) than the definite arc of a wheel (need coordinated movements along two axes).
- The velocity of the grinding wheel is parallel to that of the workpiece, which is beneficial to the improvement of surface roughness [7].

The grinding characteristics of the three different modes shown in Fig. 1 are summarised in Table 1 for comparison.

Table 1: Characteristics of three different grinding modes

| **Grinding mode** | **Perpendicular mode** | **Inclined axis mode** | **Single point inclined axis mode** |
|---|---|---|---|
| *Inclined angle of spindles of wheel and workpiece* | Perpendicular | 45 degree in *YOZ* plane | Variable |
| *Grinding wheel* | Arc shape, large arc radius, | Arc shape, arc radius > 0.1 mm, | Cube corner, whose radius can reach 0.005 mm |

| *Control centre* | Contact Point | Centre of grinding wheel | Grinding tip |
|---|---|---|---|
| *Positioning controlling* | Easy | Difficult | Easy |
| *Controlling axis* | *X-Z* axes | *X-Z* axes | *X-Z-B* axes |
| *Truing* | Difficult | Difficult | Easy |

## 3. Geometrical determination and truing/dressing of a grinding wheel

### 3.1 Determination of radius of a cylindrical wheel

In profile grinding of concave surface, the diameter of the wheel will influence the interference between the wheel and the workpiece. As shown in Fig. 2(a), a small cylindrical wheel moves along the line $OP_3$ to generate an axisymmetric surface. The bottom of the wheel may intersect with the workpiece surface if its diameter is sufficiently great. In this case, the intersection curve is $P_1PP_2$. In single point inclined axis grinding, the wheel end face is kept to have an angle of $45^o$ with the perpendicular

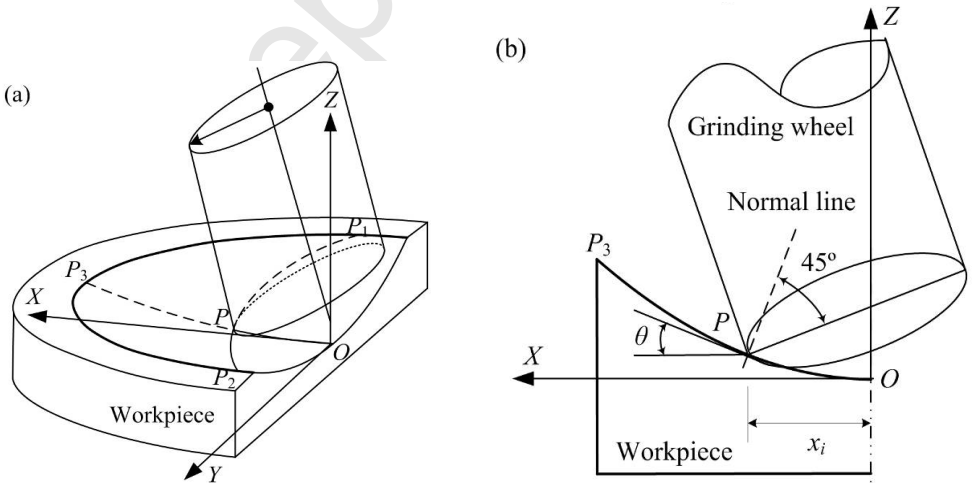

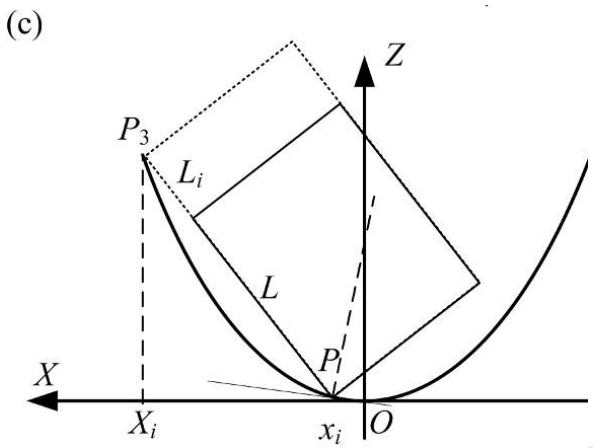


Fig. 2: Schematic illustration of (a) grinding positions of a cylindrical wheel and a concave surface (3D view), (b) the interference of the wheel and the surface along radial direction (cross-sectional view), and (c) the interference of the wheel and the surface along length direction (cross-sectional view).

line at the contact point $P$. Assuming that the curvature radius is $R_i$ at the point $P$ and the radius of cylinder grinding wheel is $R$, the curve $OP_3$ of the aspheric surface can be written as[26],

$$f(x)=\frac{x^2}{R_{base}+\sqrt{R_{base}^2-(1+k)x^2}}+\sum_{j=2}^{m}A_{2j}x^{2j} \tag{1}$$

where $x$ is the coordinate of the aspheric profile in $X$-axis, $R_{base}$ is the base radius of the profile curvature, $m$ is equal to 5 in this work, $k$ is the conic constant and $A_{2j}$ are the aspheric deformation constants.

As shown in Fig. 2(b), the angle, $\theta$, between the tangential vector at point $P$ ($x = x_i$) and $X$-axis is defined as arctan ($f'(x_i)$), and the intersection curve of $P_1PP_2$, shown in Fig. 2(a) is expressed as,

$$\begin{cases} F(x,y,z)=z-f'(x_i)+(x-x_i)\tan(45^\circ-\theta) \\ G(x,y,z)=z-\dfrac{x^2+y^2}{R_{base}+\sqrt{R_{base}^2-(1+k)(x^2+y^2)}}-\sum_{j=2}^{m}A_{2j}(x^2+y^2)^j \end{cases} \tag{2}$$

where $y$ and $z$ are the coordinate values of the aspheric profile in $Y$ and $Z$ axes, respectively. $F(x,y,z)$ is a implicit function of the bottom plane surface of grinding wheel in coordinate system $OXYZ$. $G(x,y,z)$ is another implicit function of the aspheric surface in the same coordinate system. The intersection curve of two surfaces is $P_1PP_2$. $f'(x_i)$ is a derivative value of equation $f(x)$ at point $P(x=x_i)$. The curvature radius of $P_1PP_2$ at point $P$ is calculated as:

$$R_i = \frac{\left|\boldsymbol{Q}\times\boldsymbol{S}\right|^3}{\left|M\boldsymbol{Q}-N\boldsymbol{S}\right|} \tag{3}$$

where $\boldsymbol{Q}=\left(\frac{\partial F}{\partial x},\frac{\partial F}{\partial y},\frac{\partial F}{\partial z}\right)$, $\boldsymbol{S}=\left(\frac{\partial G}{\partial x},\frac{\partial G}{\partial y},\frac{\partial G}{\partial z}\right)$,

$$M=\frac{\partial^2 G}{\partial x^2}\alpha^2+2\frac{\partial^2 G}{\partial y\partial x}\alpha\beta+2\frac{\partial^2 G}{\partial z\partial x}\alpha\gamma+\frac{\partial^2 G}{\partial y^2}\beta^2+2\frac{\partial^2 G}{\partial z\partial y}\beta\gamma+\frac{\partial^2 G}{\partial z^2}\gamma^2$$

$$N=\frac{\partial^2 F}{\partial x^2}\alpha^2+2\frac{\partial^2 F}{\partial y\partial x}\alpha\beta+2\frac{\partial^2 F}{\partial z\partial x}\alpha\gamma+\frac{\partial^2 F}{\partial y^2}\beta^2+2\frac{\partial^2 F}{\partial z\partial y}\beta\gamma+\frac{\partial^2 F}{\partial z^2}\gamma^2$$

$$\alpha=\frac{\partial F}{\partial y}\frac{\partial G}{\partial z}-\frac{\partial F}{\partial z}\frac{\partial G}{\partial y},\quad \beta=\frac{\partial F}{\partial z}\frac{\partial G}{\partial x}-\frac{\partial F}{\partial x}\frac{\partial G}{\partial z},\quad \gamma=\frac{\partial F}{\partial x}\frac{\partial G}{\partial y}-\frac{\partial F}{\partial y}\frac{\partial G}{\partial x}$$

If the curvature radius, $R_i$, is greater than $R$ at the grinding point $P$ ($x = x_i$), then interference can be avoided. By using this method, the value of $R_i$ at every grinding point from the centre to the side was calculated. The minimum value of radius $R$ is thus found, which prevents the cylindrical grinding wheel from interfering with the aspheric surface, i.e. we have to make sure:

$$R < \min\left\{R_0,\ R_1,\cdots,R_i,\cdots,R_n\right\} \tag{4}$$

Where, $n$ is the number of grinding point in X-axis direction. Fig. 3(a) and Fig. 3(b) show the relationships of the interference radius of the cylindrical wheel and the $X$-axis position of a concave surface with the aspheric parameters shown in Table 2. The

maximum radii of the wheel are 1.12 mm and 5.15 mm for grinding the 2 mm and 6 mm moulds, respectively.

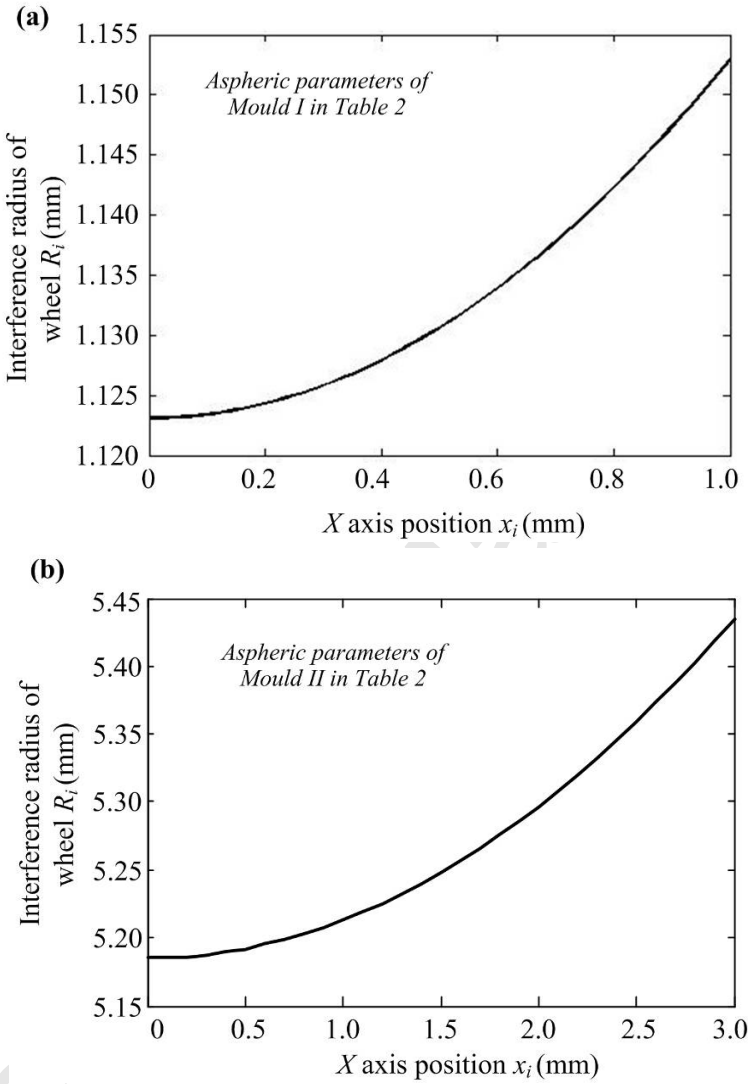


Fig. 3: Radius of the cylindrical wheel for non-interference is plotted against the X-axis position for grinding the moulds of (a) 2 mm and (b) 6 mm in aperture diameter.

Table 2: Geometric parameters of the aspheric surface

| Parameter | Mould I | Mould II |
|---|---|---|
| Base radius, $R_{base}$ (mm) | 1.588 | 7.333 |
| Aperture diameter (mm) | 2 | 6 |

| | | |
|---|---|---|
| $k$ | -0.1367 | -0.72 |
| $A_4$ | 5.426e-5 | 4.42e-5 |
| $A_6$ | 1.382e-8 | 8.38e-8 |
| $A_8$ | -6.434e-10 | -6.43e-10 |
| $A_{10}$ | -9.726e-12 | -9.72e-12 |

3.2 Determination of length of a cylindrical wheel

As shown in Fig. 2(c), if the cylindrical wheel is too long, the interference between the wheel and the workpiece can also be caused. Assume that $L$ is the maximum length of the wheel and $L_i$ represents the interference length at any grinding point of $P$, during grinding $L$ must be smaller than $L_i$, so the interference can be avoided. The intersection points of Line $PP_3$ and the aspheric profile, $f(x)$, can be obtained by

$$f(X_i) - f(x_i) = \tan(\arctan(f'(x_i)) + 45^\circ)(X_i - x_i) \quad (5)$$

If interference occurred, $X_i$ could be obtained using the Newton iteration method. The maximum length $L$ could thus be obtained by calculating every grinding point from the centre point to the outer using this method:

$$L < \min\{L_0, L_1, \cdots, L_i, \cdots, L_n\} \quad (6)$$

In this work, no interference would occur for the grinding the 2 and 6 mm moulds shown in Table 2.

3.3 Truing and dressing of the grinding wheel

The cylindrical surface and end face of grinding wheel must be trued to obtain a cube corner cutting edge. In this work, a truing wheel was installed on the workpiece spindle, which is also cylindrical, but with larger diameter and coarser abrasives than the grinding wheel being trued, as shown in Fig. 4(a). When truing the cylindrical surface,

once the two surfaces were in contact, the truer was moved following the path: *X*-axis feeding, *Z*-axis truing, *Z*-axis retracting and *X*-axis feeding. When truing the end face, the grinding wheel was moved following the path: Z-axis feeding, *X*-axis truing, *Z*-axis feeding and *X*-axis truing. Both processes were repeated until satisfactory result was achieved. Fig. 4(b) shows the cube corner of the trued wheel. The radius of the wheel corner was estimated to be 5μm. Detailed truing conditions can be found from Table 3. Dressing was carried out by grinding a dummy workpiece using the same conditions as those used in the grinding (see Table 4) for 3 minutes.

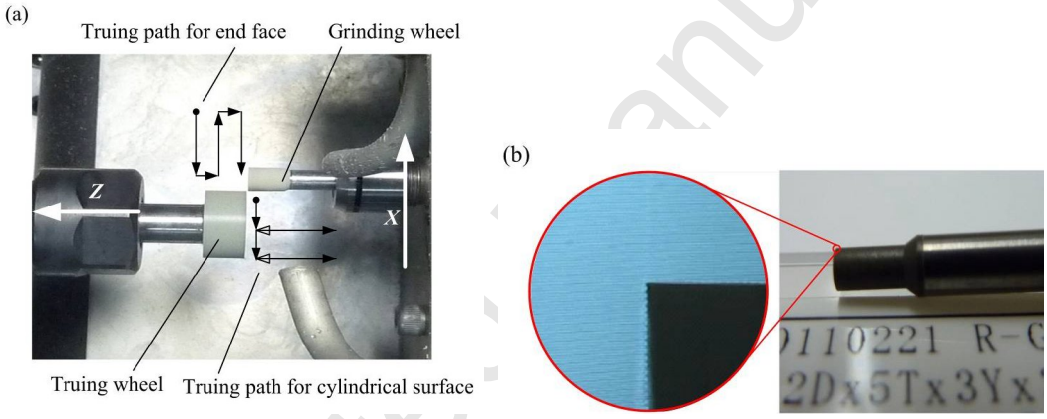


Fig. 4: (a) Set-up for truing the cylindrical surface and end face of a resin bond diamond wheel and (b) the enlarged optical image of the wheel corner achieved.

Table 3: Truing and dressing conditions

| Grinding wheel | Resin bond, mesh #2000, 2 mm and 6mm in diameter |
|---|---|
| Truing: Diamond truer of mesh size of 600 | |
| Work rotation (r/min) | 200 |
| Wheel rotation (r/min) | 45000 |
| Cutting depth (μm) | 1 |
| Feed rate (mm/min) | 1 |
| Cool fluid | water soluble |
| Dressing: The wheel grinds a dummy workpiece using the same conditions as those used in the grinding for 3 minutes. | |

## 4. Error analysis and compensation grinding approach

### 4.1 Analysis of major error sources

#### 4.1.1 Positioning offset along radial direction (X-axis)

To generate an axisymmetric surface, a grinding wheel must move along both radial (*X*-axis) and axial (*Z*-axis) directions from the workpiece centre. If the wheel cannot position right at the centre, a 'Λ-shaped' or 'V-shaped' residue will be left on the machined surface due to the setting error of position, which can significantly decrease the profile accuracy. An offset inward will generate a V-shaped profile at the centre, as shown in Fig. 5(a), and an offset outward will leave a Λ-shaped profile, as shown in Fig. 5(b). During grinding a concave aspheric surface, the profile error is directly related to the setting error of the wheel, as shown in Fig. 5(c), which can be expressed as:

$$f(x_i - e_x) + e_i = f(x_i) \tag{7}$$

Where $e_x$ is the setting error, $e_i$ the measured profile error at an arbitrary point $T_i$, $x_i$ is the *X*-axis coordinate value at point $T_i$. Thus, the setting error at point $T_i$ could be obtained by iteratively calculating Eq. (7) using the Newton's Iteration method.

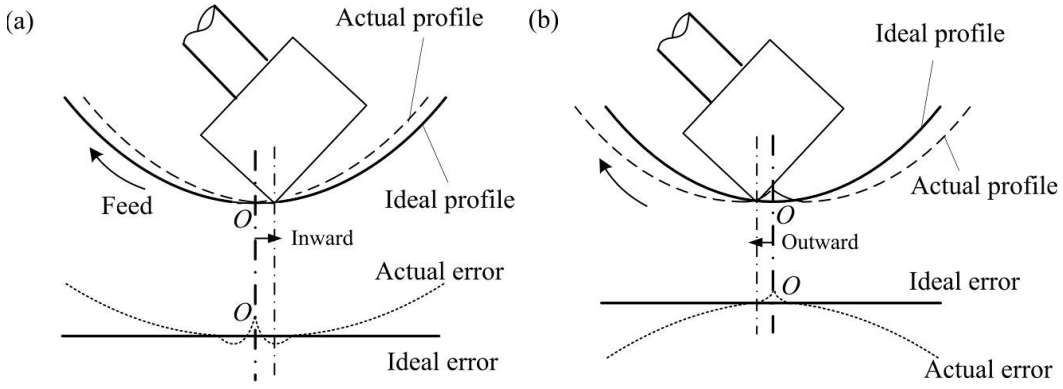

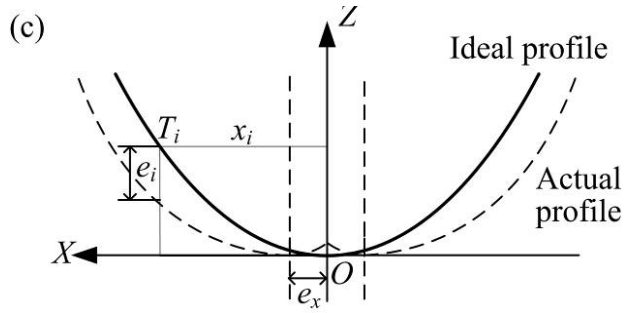


Fig. 5: Schematic illustration of profile errors caused by (a) inward offset and (b) outward offset along radial (or *X*-axis) direction of a grinding wheel with respect to the workpiece, and (c) calculating setting error.

4.1.2 Tool wear

As the grinding is carried out via point contact via a very sharp corner, the tool wear is significant in this grinding mode. Fig. 6 schematically illustrates the wear of the grinding wheel in the middle of grinding, where the corner tip of the cylindrical wheel in fact became a small arc. This will result in the significant profile error in the aspheric surface being generated. The tool wear and arc shape could be estimated by subtracting the ideal profile from the measured profile after grinding. After compensating the positioning error, the difference in profile along *Z*-axis is assumed mainly due to the tool wear.

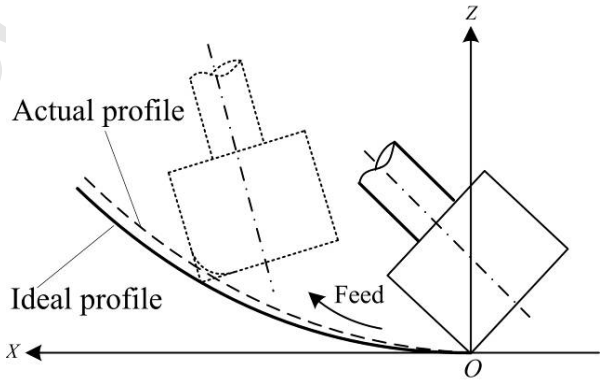


Fig. 6: Profile error caused by the wheel wear.

4.2 Compensation grinding protocol

As tool wear and positioning offset are expected to be the two major error sources, which would significantly affect the profile accuracy in single point inclined axis grinding, error compensation module is integrated into the grinding protocol. The setting error must be present after installing the fine grinding wheel. The shape of error profile is greatly affected by the positioning offset and it is an obvious Λ shape or V shape. In general, the compensation of positioning offset should be carried out if the PV value is about over 600 nm. After compensating the positioning error, the shape of error profile mainly affected by the tool wear is a regular slight fluctuation. If form error is about below 600 nm, the compensation of tool wear will be processed to generate new grinding path. As shown in Fig. 7, at first the workpiece was roughly ground using a grinding wheel of mesh size of 350 to rapidly form the aspheric surface. After that, a small superfine grinding wheel of mesh size of 2000 was carefully trued into the required wheel shape and dressed properly prior to grinding. The surface was then finely ground along the ideal grinding path generated using the shape parameters in Table 2.

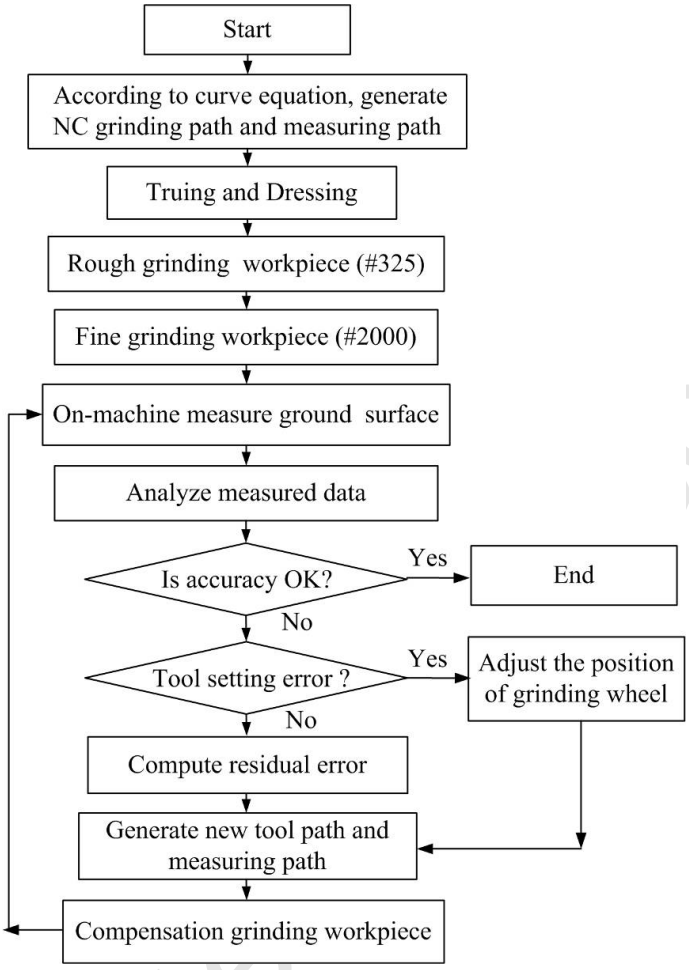


Fig. 7: Protocol of the compensation grinding.

The ground profile was measured using the on-machine probing. The measured profile data was filtered to remove high-frequency random error prior to analysis. According to the shape of the profile error curve, the effect of positioning offset and tool wear could be identified and distinguished in order to determine the compensation approach. If the profile error was mainly derived from the tool setting error, it should be firstly compensated through adjusting the positioning of the grinding wheel based on the error analysis shown in Fig. 5. If the main error was derived from tool wear, a new tool path would be generated through superimposing the filtered error with ideal ground profile, fitting the actual grinding and calculating normal residual error. As shown in Fig.

8, the coordinates of the new ground point after compensation, ($X_{2i}$, $Z_{2i}$), and the rotation angle of the grinding wheel, $\theta_i$, can be expressed as [6],

$$\begin{aligned} X_{2i} &= X_{1i} + E\sin\theta_i \\ Z_{2i} &= Z_{1i} - E\cos\theta_i \end{aligned} \tag{8}$$

where ($X_{1i}$, $Z_{1i}$) are the coordinates of Point $P$ on the target profile, $E$ is the distance between Point $P$ and the corresponding point at the actual profile along $\mathbf{n}_i$ that is a normal vector of Point $P$. Once the new tool path, i.e. ($X_{2i}$, $Z_{2i}$), is determined, compensation grinding can be performed. The procedures were repeated three or four time until the profile accuracy met the requirement.

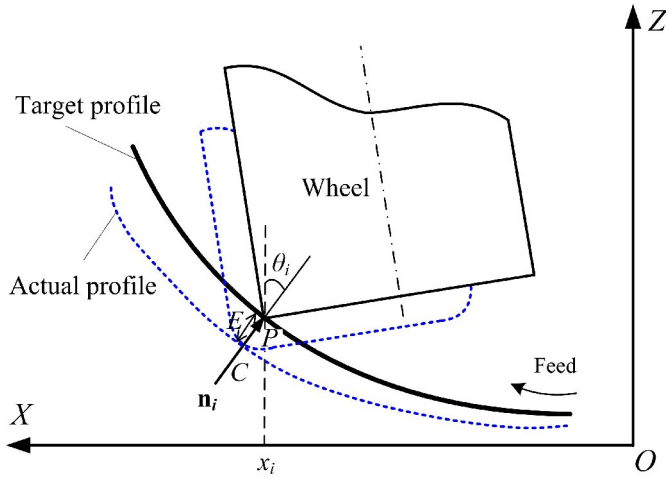


Fig. 8: Illustration of determination of compensation path.

## 5. Grinding experiments and results

### 5.1 Experimental details

Grinding experiments were performed on a 4-axis ultraprecision grinding centre with on-machine profile measurement, as shown in Fig. 9. The machine has a linear resolution of 1 nm in $X$- and $Z$- axes. The resolution of rotary movement around $B$-axis is $0.0001^{o}$. The workpiece was installed on a vacuum chuck and the workpiece spindle can also move vertically along the $Y$-axis. The grinding spindle was placed on the $B$-axis rotary platform. The $B$-axis rotary platform and the on-machine measurement

device were both installed on the *X*-axis platform. The on-machine probing system has been calibrated after integrating on the ultra precision machine tool by NACHI. The resolution is 1nm, and the straightness accuracy is below 0.20 μm/300 mm. The radius of the measuring probe is 0.25 mm. The contact force is 0.53N and the measuring angle is ±60 degree. It has the same position accuracy as the ultra-precision machine tool. The on-machine measurement was in excellent agreement with the off-machine measurements by the commercially available precision profilometer[5].

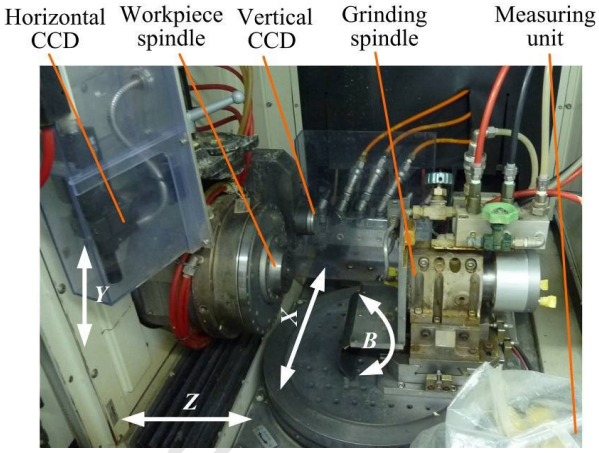


Fig. 9: Illustration of grinding set-up.

Tungsten carbide was the mould material being machined. Two concave aspheric surfaces were generated with apertures of 2 mm and 6 mm, respectively. The detailed geometric parameters of the two aspheric surfaces are shown in Table 2.

Cylindrical grinding wheels of 2 and 6 mm in diameter were selected for grinding the aspheric surfaces with apertures of 2 mm and 6 mm, respectively. Diamond wheels of with cast iron bond of #325 and resin bond of #2000 were employed for rough and fine grinding. The rough grinding aimed to take bulk removal of material, but the fine grinding targeted at achieving the required profile accuracy. Prior to fine grinding, the cylindrical and end face of the grinding wheel was precisely trued using a diamond truer of mesh size of 600 using the conditions shown in Table 3. Dressing was completed by

grinding a dummy workpiece for 3 minutes using the same grinding conditions listed in Table 4.

Table 4: Grinding conditions

| | Rough grinding | Fine grinding | | |
|---|---|---|---|---|
| | | 1st cycle | 2nd cycle | 3rd cycle |
| Diamond wheel | Cast iron, mesh #325 | Resin bonded, mesh #2000 | | |
| Work rotation (r/min) | 200 | 150 | | |
| Wheel rotation (r/min) | 45000 | 45000 | | |
| Pitch (μm) | 2 | 2 | | |
| Cutting depth (μm) | 2 | 1 | 1 | 0.5 |
| Feed rate (mm/min) | 5 | 1 | 1 | 0.5 |
| Cool fluid | NK-Z water soluble fluid 1: 20 | | | |

5.2 Results and discussion

Fig. 10 shows the profile error curves of the 2 mm mould ground using the single point inclined axis mode. The first fine grinding was done without error compensation, which has a profile error of 1034 nm in peak-to-valley (PV) value obtained from the on-machine measurement, as shown in Fig. 10(a). The "V-shaped" profile in error curve is obvious, indicating that the setting offset of the wheel was inward. Thus in the next grinding cycle, the position of the wheel was adjusted in *X*-axis and the wear error in *Z*-axis was compensated in the new tool path. After the second fine grinding with error compensation, the profile accuracy was improved to 489 nm in PV (and 108 nm in RMS). From the error curve shown in Fig. 10(b), the setting error is not obvious, but the errors are fluctuated with a magnitude of less than 0.5 μm along the radial direction (*X*-axis). To further improve the accuracy and avoid overcompensation, the compensation procedure was repeated by setting a weighting ratio to 70%. After the third fine grinding, the profile accuracy was improved to 146 nm in PV (and 25 nm in

RMS), as shown in Fig. 10(c).

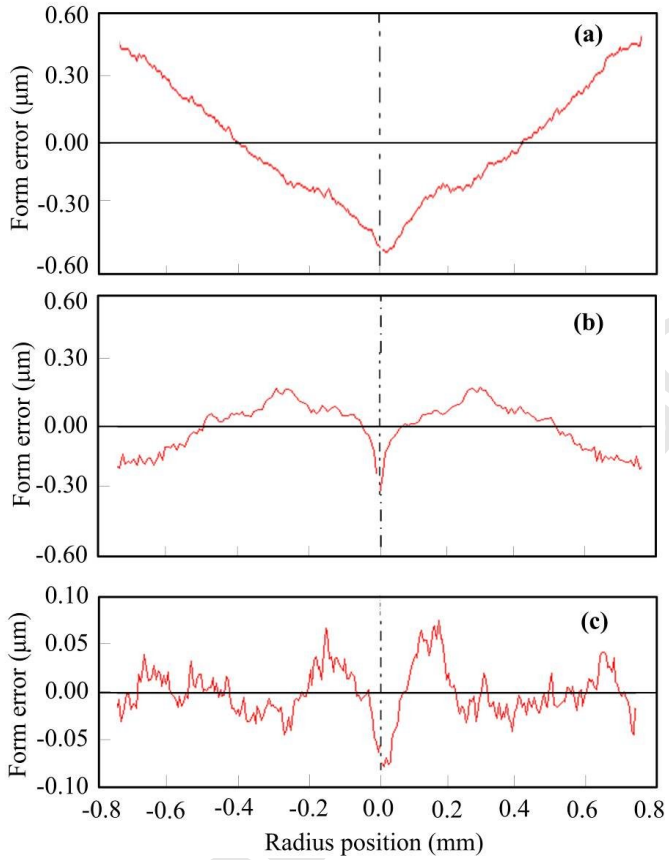


Fig. 10: Profile error curve of the 2 mm mould (a) after 1st fine grinding cycle with 1034 nm in PV, (b) after 2nd grinding cycle with 489 nm in PV and (c) after 3rd grinding cycle with 146 nm in PV.

Fig. 11 shows the profile error curves of the 6 mm mould ground using the same grinding procedure described earlier. As shown in Fig. 11(a), the error of 1293 nm in PV was obtained after the first grinding cycle that was without compensation. After adjusting the centre position and compensating the tool wear in the new tool path, the profile error after the second grinding was decreased to 449 nm in PV (shown in Fig. 11(b)). After the third grinding cycle, the form accuracy was improved to 323 nm PV, as shown in Fig.11(c). To meet the required profile accuracy of below 200 nm, the fourth grinding cycle was employed, which further reduced the profile error to 182 nm as shown in Fig. 11(d).

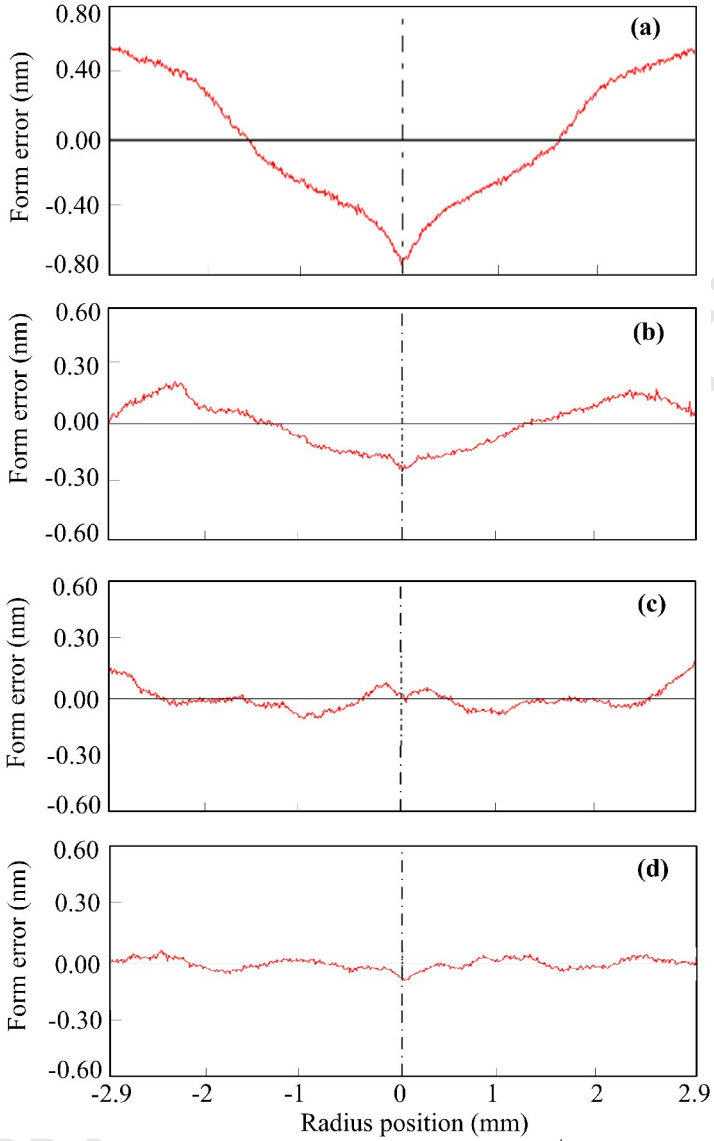


Fig. 11: Profile error curve of the 6 mm mould (a) after 1st fine grinding cycle with 1293 nm in PV, (b) after 2nd grinding cycle with 449 nm in PV, (c) after 3rd grinding cycle with 323 nm in PV and (d) after 4th grinding cycle with 182 nm in PV.

Fig. 12 shows the profile errors achieved after each fine grinding cycle for the two moulds being ground. As can be seen from this figure, profile accuracy of below 200 nm in PV value could be obtained after 3 or 4 fine grinding cycles or 2 or 3 compensation grinding cycles. For the larger mould, one more cycle was used. This could be because more significant tool wear occurred than the estimated value during

the grinding of this mould, so the weighting ratio for compensation set up in the 2nd compensation grinding cycle was insufficiently great.

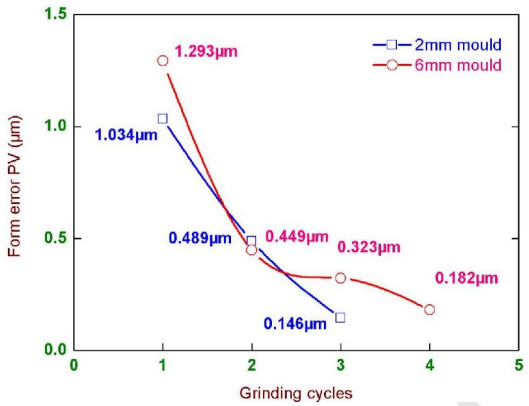


Fig. 12: Profile errors of the 2 and 6 mm moulds after fine grinding plotted as a function of grinding cycle.

Fig. 13 shows typical images of topography of the two ground aspheric surfaces measured by a white light interferometer (Zygo: New View 5032). The average surface roughness values obtained after the final grinding process were 2.2 and 1.8 nm for the 2 and 6 mm moulds, respectively. Fig. 14 demonstrated that the surfaces of the two moulds are with mirror surface finish.

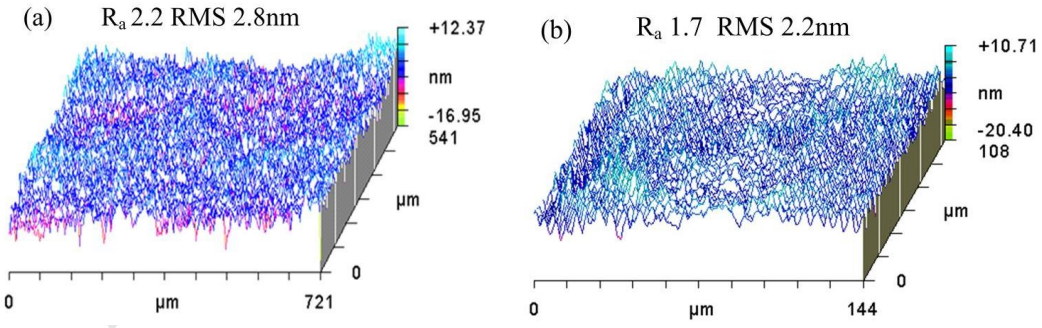


Fig. 13: Surface roughness of the two moulds of (a) 2 mm and (b) 6 mm in aperture diameter.

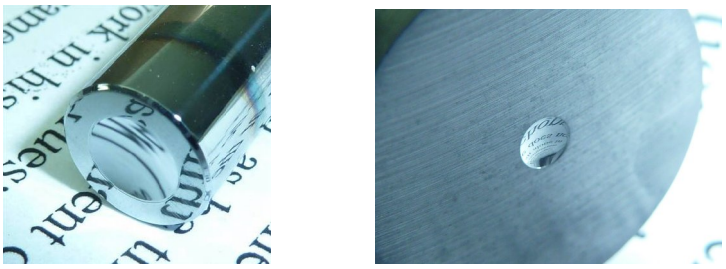

(a) (b)

Fig. 14: Optical images of the (a) 2 mm and (b) 6 mm moulds after single point inclined axis grinding, showing mirror surface finish.

## 6. Conclusions

The interference of a cylindrical grinding wheel with the workpiece in single point inclined axis grinding of small concave surface was analysed and the criteria for selection of wheel geometry for avoiding the interference was set up. The grinding protocol with compensation focusing on tool setting error and tool wear was developed based on comprehensive error analysis. The grinding performance demonstrated that in this grinding process, the tool setting error and wheel wear was indeed the two major error sources. The results also showed that the grinding process was capable to generate small aspheric concave surfaces on tungsten carbide material that has high accuracy with a profile error of smaller than 200 nm in PV value.

## Acknowledgements

This work was sponsored by the NSFC (51205120), the International Science & Technology Cooperation Program of China (2012DFG70640) and Young Teacher Plan of Hunan University. HH is financially supported by Australia Research Council (ARC).

**References**

[1] Yin SH, Ohmori H, Dai YT, Uehara Y, Chen FJ, Tang HN. ELID grinding characteristics of glass-ceramic materials. International Journal of Machine Tools and Manufacture 2009;49:333–338.

[2] Lin Y, Huang H. Brittle materials in nano-abrasive fabrication of optical mirror-surfaces. Precision Engineering 2008;32:336-341.

[3] Ohmori H, Nakagawa T. Analysis of mirror surface generation of hard and brittle materials by ELID (Electronic In-Process Dressing) grinding with superfine grain metallic bond wheels. CIRP Annals-Manufacturing Technology 1995;44: 287-290.

[4] Brinksmeier E, Mutluguenes Y, Klocke F, Aurich JC, Shore P, Ohmori H. Ultra-precision grinding. CIRP Annals-Manufacturing Technology 2010;59: 652-671.

[5] Chen FJ, Yin SH, Huang H, Ohmori H, Wang Y, Fan YF, Zhu YJ. Profile error compensation in ultra-precision grinding of aspherical surfaces with on-machine measurement. International Journal of Machine Tools and Manufacture 2010;50 480-486.

[6] Chen FJ, Yin SH, Ohmori H, Yu JW. Form error compensation in single-point inclined axis nanogrinding for small aspheric insert. International Journal of Advanced Manufacturing Technology 2012;65: 433-441.

[7] Chen WK, Huang H, Yin L. Machining of micro aspherical mould inserts. Precision Engineering 2005;29: 315-323.

[8] Cha DH, Kim HJ, Lee JK, Kim HU, Kim SS, Kim JH. A study of mould grinding and pressing conditions in the moulding of aspherical glass lenses for camera phone module. Materials and Manufacturing Processes 2008;23: 683-689

[9] Han JY, Kim SW, Han I, Kim GH. Evolutionary grinding model for nanometric control of surface roughness for aspherical optical surfaces. Optics Express 2008;16: 3786-3797.

[10] Kim HT, Yang HJ, Kim SC. Sub-micron control algorithm for grinding and polishing aspherical surface. International Journal of Control, Automation, and Systems 2008;6:386-393.

[11] Ohmori H. Electrolytic in-process dressing (ELID) grinding technique for ultraprecision mirror surface machining. Journal of the Japan Society for Precision Engineering 1992;26: 273–278. [in Japanese language].

[12] Xie J, Zhou RM, Xu J, Zhong YG. Form-truing error compensation of diamond grinding wheel in CNC envelope grinding of free-form surface discharge process. International Journal of Advanced Manufacturing Technology 2010;48: 905-912.

[13] Ortega N, Pombo I, Sanchez JA, Izquierdo B, Alberdi SPR. Electrodischarge dressing (EDD) applied to contour grinding. International Journal of Mechatronics and Manufacturing Systems 2010; 3:345-356.

[14] Sanchez JA, Pombo I, Cabanes I, Ortiz R, Lopez de Lacalle LN. Electrical discharge truing of metal-bonded CBN wheels using single-point electrode. International Journal of Machine Tools and Manufacture 2008;48: 362-370.

[15] Marsh ER, Moerlein AW, Deakyne TRS, Van Doren MJ. In-process measurement of form error and force in cylindrical-plunge grinding. Precision Engineering 2008;32: 348-352

[16] Huang H, Chen WK, Kuriyagawa T. Profile error compensation approaches for parallel nano-grinding of aspherical mould inserts. International Journal of Machine Tools and Manufacture 2007;47: 2237-2245.

[17] Rao VS, Rao PVM. Tool deflection compensation in peripheral milling of curved geometries. International Journal of Machine Tools and Manufacture 2006;46: 2036-2043.

[18] Suzuki H, Tanaka K, Takeda H, Kawakami K, Nishioka M. Study on precision grinding of micro aspherical surface (2nd report)—effects of tool errors on workpiece form accuracies and its compensation methods. Journal of the Japan Society for Precision Engineering 1998;64: 1211–1215. [in Japanese language].

[19] Yi L, Funkenbusch PD, Gracewski SM, Ruckman J. Tool wear and profile development in contour grinding of optical components. International Journal of Machine Tools and Manufacture 2004;44: 427-438

[20] Gunawardane SDGSP, Yokouchi H. On the snagging operation: Part I: Modeling and simulation of wheel wear characteristics. Precision Engineering 2004;28:261-269

[21] Katsushi F, Nguyen TH, Noriyuki O, Takashi N. Automatic compensation for grinding wheel wear by pressure based in-process measurement in wet grinding. Precision Engineering 2003;27: 9-13

[22] Hsu YY, Wang SS. A new compensation method for geometry errors of five-axis machine tools. International Journal of Machine Tools and Manufacture 2007;47: 352-360.

[23] Rahman M, Heikkala J, Lappalainen K. Modeling, measurement and error compensation of multi-axis machine tools. Part I: theory, International Journal of Machine Tools and Manufacture 2000;40: 1535-1546.

[24] Pereira PH, Giacomo BD. Thermal error evaluation and modeling of a CNC cylindrical grinding machine. Metrologia. 2008;45: 217-222.

[25] Tian Y, Shirinzadeh B, Zhang D, Liu X, Chetwynd D. Effects of the heat source profiles on the thermal distribution for ultraprecision grinding. Precision Engineering 2009;33: 447-458.

[26] Ohumil J. Optical Surfaces, first ed., New York: Elsevier Science Ltd, 1976.

**Figure and Table Captions**

Fig. 1: Schematic illustration of three different grinding modes: (a) perpendicular mode, (b) inclined axis mode using an arc wheel and (c) single point inclined axis mode.

Fig. 2: Schematic illustration of (a) grinding positions of a cylindrical wheel and a concave surface (3D view), (b) the interference of the wheel and the surface along radial direction (cross-sectional view), and (c) the interference of the wheel and the surface along length direction (cross-sectional view).

Fig. 3: Radius of the cylindrical wheel for non-interference is plotted against the X-axis position for grinding the moulds of (a) 2 mm and (b) 6 mm in aperture diameter.

Fig. 4: (a) Set-up for truing the cylindrical surface and end face of a resin bond diamond wheel and (b) the enlarged optical image of the wheel corner achieved.

Fig. 5: Schematic illustration of profile errors caused by (a) inward offset and (b) outward offset along radial (or *X*-axis) direction of a grinding wheel with respect to the workpiece, and (c) calculating setting error.

Fig. 6: Profile error caused by the wheel wear.

Fig. 7: Protocol of the compensation grinding.

Fig. 8: Illustration of the determination of new compensation path.

Fig. 9: Illustration of the grinding set-up.

Fig. 10: Profile error curve of the 2 mm mould (a) after 1$^{st}$ fine grinding cycle with 1034 nm in PV, (b) after 2$^{nd}$ grinding cycle with 489 nm in PV and (c) after 3$^{rd}$ grinding cycle with 146 nm in PV.

Fig. 11: Profile error curve of the 6 mm mould (a) after 1$^{st}$ fine grinding cycle with 1293 nm in PV, (b) after 2$^{nd}$ grinding cycle with 449 nm in PV, (c) after 3$^{rd}$ grinding cycle with 323 nm in PV and (d) after 4$^{th}$ grinding cycle with 182 nm in PV.

Fig. 12: Profile errors of the 2 and 6 mm moulds after fine grinding plotted as a function of grinding cycle.

Fig. 13: Surface roughness of the two moulds of (a) 2 mm and (b) 6 mm in aperture

diameter.

Fig. 14: Optical images of the (a) 2 mm and (b) 6 mm moulds after single point inclined axis grinding, showing mirror surface finish.

Table 1: Characteristics of three different grinding modes
Table 2: Geometric parameters of the aspheric surface
Table 3: Truing and dressing conditions
Table 4: Grinding conditions

## Highlights

► A single point inclined axis grinding protocol was developed for fabrication of aspheric moulds, which enabled improved profile accuracy.
► The selection criteria of cylindrical wheels for avoiding the interference were proposed.
► The compensation method focused on centering and tool wear error was developed and proven to be effective